Use of a stealth boundary with finite difference frequency domain simulations of simple antenna problems

R.B. Thompson, F.S. Chute, and F.E. Vermeulen

Department of Electrical Engineering
University of Alberta
Edmonton, Alberta, Canada T6G 2G7
(403) 492-3332

Abstract

A direct method for the numerical solution of Maxwell's equations in the frequency domain (sinusoidal steady state), for radiation problems of cylindrical symmetry, is incorporated into a finite difference program called HERZ, coded in FORTRAN. The termination of the fields on the outer boundary of the problem domain is accomplished *via* an absorptive layer, labelled a *stealth layer*, which attenuates the incident fields to insignificant amounts in a small computing space, without causing significant reflections that would disturb the near field solutions. No radiation boundary condition is specified on the problem domain, rather, the transmission of the fields to the stealth layer is optimized by specifying its electrical properties. To validate HERZ as a useful electromagnetic modeller for thin wire antennas, driving point admittances and surface current distributions for several configurations were compared to both theoretical and measured values, with good agreement.

Introduction

In the numerical modeling of radiation problems, particularly those of isolated thin wire antennas, specific radiation boundary conditions allow finite difference or finite element techniques to be applied (Ramahi *et al.* 1991). The implementation of non-local boundary conditions such as boundary integral formulations or moment method techniques is useful for infinite homogeneous configurations but bounded methods are typically incorporated in conjunction with these techniques if inhomogeneities exist, such as in the case of a dielectrically coated antenna (McDonald and Wexler 1972, Morgan *et al.* 1984, Yuan *et al.* 1990). To avoid the complication of coupling a bounded problem to an unbounded problem, specific radiation boundary conditions are formulated in conjunction with finite element techniques (Sumbar *et al.* 1990).

While finite element techniques allow for very flexible grid density and are straightforward in their treatment of inhomogeneites, the complex nodal grids which must be generated lack the physical transparency and simplicity of a finite difference grid system. In this paper an absorbing layer adjacent to the problem space boundary is used in place of an explicit radiation boundary condition. Rather than specifying a radiation condition to terminate the fields of the antenna, shown in Fig. 1, on the problem domain, the transmission of the fields from the problem domain to a lossy layer enveloping the problem domain is modelled, as illustrated in Fig. 2. The problem domain's boundaries are then in an interior grid location, as the grid encompasses both the problem domain and it's surrounding lossy layer, which will now be referred to as the *stealth layer*. The near-field problem can then be solved at the expense of the far-field solutions, which will be attenuated in the stealth layer, without disturbing the field distributions within the initial problem domain. A related technique for truncating the solution domain in finite element scattering problems has been discussed in the literature (Jin *et al.* 1991, 1992).

This methodology is incorporated into a FORTRAN program, called HERZ (H field E field, R - Z geometry), which is executed on a Macintosh II personal computer. The finite difference implementation of Maxwell's equations and the use of the absorptive stealth layer are described in the following sections. Several antenna configurations are modelled with HERZ to validate this approach, comparing field related values such as driving point admittances and surface current distributions to published theoretical and measured results.

Finite difference implementation of Maxwell's equations

Cylindrically symmetric metallic antennas operating in cylindrically symmetric inhomogeneous materials, with geometries as shown in Fig. 1, will have simplified electric and magnetic field orientations when the electrical properties of these materials are isotropic. The electric fields will have radial and axial components (r,z), and the magnetic fields only an azimuthal component (ø).

The general time-harmonic solutions will be of the form

$$\mathbf{E} = E_r(r,z)\hat{\mathbf{a}}_r + E_z(r,z)\hat{\mathbf{a}}_z \quad (1)$$

$$\mathbf{H} = H_\phi(r,z)\hat{\mathbf{a}}_\phi. \quad (2)$$

Assuming an $e^{j\omega t}$ time dependence, the integral form of Maxwell's equations can be expressed as

$$\oint \mathbf{E}\cdot\mathbf{dl} = -j\omega\mu\iint \mathbf{H}\cdot\mathbf{dS} \quad (3)$$

and

$$\oint \mathbf{H}\cdot\mathbf{dl} = (\sigma + j\omega\varepsilon)\iint \mathbf{E}\cdot\mathbf{dS}\,. \quad (4)$$

The solution technique adopted uses these integral equations to form surfaces and contours accommodated by the finite difference grid structure (Albani and Bernardi 1974), providing an algorithm to compute the azimuthal magnetic field component, H_ϕ, at the center of every gridblock. (3) was discretized to express the H_ϕ field in a gridblock center in terms of the four E field values which surround it, as is displayed in Fig. 3, the finite difference grid implementation in HERZ. The resulting linear equation is of the form

$$a_{i,j}\,E_{zi,j} + b_{i,j}\,E_{ri,j+1} + c_{i,j}\,E_{zi+1,j} +$$

$$d_{i,j}\,E_{ri,j} = e_{i,j}\,H_{\phi' i,j} \quad (5)$$

where the coefficients $a_{i,j}$ to $e_{i,j}$ depend on the grid dimensions Δr_i and Δz_j (Nachai *et al.* 1992). The gridblocks have been assumed to be small enough that the electric field components are constant along each line segment of the gridblock i,j and the magnetic field is uniform over its cross section. In this equation

$$r\,H_\phi = H_{\phi'}$$

where r is the radial distance to the center of the gridblock where H_ϕ is being calculated.

By applying (4) to appropriate surfaces and contours, the various electric field components in (5) can be written in terms of the magnetic fields at the centers of the surrounding gridblocks. For example, with reference to Fig. 3, $E_{zi,j}$ can be expressed in terms of $H_{\phi' i-1,j}$ and $H_{\phi' i,j}$ by applying (4) to the contour consisting of two concentric circular paths of radii r_{i-1} and r_i to compute the total axial current (conduction and displacement) through the enclosed surface. The equation that results for the magnetic field is

$$A_{i,j}\,H_{\phi' i,j} + B_{i,j}\,H_{\phi' i-1,j} + C_{i,j}\,H_{\phi' i+1,j} +$$

$$D_{i,j}\,H_{\phi' i,j-1} + E_{i,j}\,H_{\phi' i,j+1} = 0 \quad (6)$$

where the coefficients $A_{i,j}$ to $E_{i,j}$ are given in terms of the frequency ω, the electrical properties σ, ε and μ and the radial locations and dimensions of the pertinent gridblocks (Nachai *et al.* 1992). The discretizations of (3) and (4) are particularly transparent and easy to implement because all electric and magnetic field components are tangential to material interfaces and the difficulties that can be encountered in handling inhomogeneous problem domains in three dimensions do not arise.

Each of the N gridblocks, referred to by indices i,j, will have an associated equation of the form of (6), providing the N unknown H fields with N linearly independent equations, resulting in a determined system. To completely specify the problem, conditions must be provided on the problem boundary. Excitation by electric fields on the grid's outer domain, the Neumann boundary condition, requires an adjustment of the LHS of (6), as one of the terms E_r or E_z in (5) is then predetermined. The excitation electric field appears on the RHS of (6).

Electric field excitation is specified exclusively on the perimeter of the problem domain, where it may, for instance, be set to zero to signify the presence of a perfectly conducting boundary. At all other locations in the problem domain the electric field excitation is zero. Magnetic field excitation may be applied at the center of any gridblock by specifying a value of H_ϕ.

The set of N equations for $H_{\phi'}$ represents a banded symmetric system which can be stored in the computer in a compressed coefficient matrix, K. The unknown values of $H_{\phi'}$, and hence H_ϕ, are obtained by Gaussian elimination. The solution H_ϕ is then used in (4) to obtain the electric field values on the perimeter of every gridblock, and simple averaging is used to obtain the values of the electric fields at the gridblock centers.

Typical grids consist of approximately 75 x 75 gridblocks, with no more than 15 gridblocks per wavelength. Blocks are chosen with a consideration of the radiation wavelength, the radius and length of the antenna being modeled, as well as the gap size used to excite the antenna.

Incorporation of stealth boundary conditions

As was stated earlier, no radiation boundary condition was directly applied at the problem domain's outer surface. Rather, optimal transmission of the fields into the stealth layer was sought. The tangential electric field at the outer boundary of the stealth layer was set to zero, which is equivalent to bounding the stealth layer with a perfect conductor.

The transmission of radiation normally incident upon a boundary is determined by the wave impedances on both sides of the material interface, with matched wave impedances providing perfect transmission. To achieve normal incidence of the radiated wave at the stealth layer, the surface of the stealth layer should be a sphere centered at the antenna, with a radius many times the wavelength. In practice it was found sufficient to approximate the surface of the sphere by a cylindrical boundary, as shown in Fig. 2, and rely upon multiple reflections from the stealth layer to minimize the disturbances to the near fields. The distance from the center of the antenna to the stealth layer's surface was set at three wavelengths. A chamfer in the stealth layer, as indicated by the dotted line in the upper right hand corner of Fig. 2, was initially used to better approximate a spherical boundary. Only a small improvement was obtained, however, at the expense of a relatively complex design. The chamfer, therefore, was not used in any of the cases considered in this paper.

The wave impedance and propagation constant for a plane wave propagating in a general lossy medium are

$$\eta = \sqrt{\frac{\mu}{\varepsilon}} = \sqrt{\frac{j\omega(\mu' - j\mu'')}{(\sigma + j\omega\varepsilon)}} \qquad (7)$$

and $$\gamma = \alpha + j\beta = \sqrt{j\omega(\mu' - j\mu'')(\sigma + j\omega\varepsilon)} \qquad (8)$$

where $\eta_{stealth} = \eta_{problem\ domain}$ would maximize transmission for normal incidence at large distances from the antenna structure, and $\alpha_{stealth}$ would define the attenuation rate in the absorbing layer. While it can be seen from Fig. 2 that waves will not impinge upon the stealth layer normal to its surface, it has been found that choosing the electrical properties to satisfy the foregoing provides satisfactory results, as exemplified by the case studies to follow. Given an excitation frequency, μ', μ'', σ, and ε in the fictitious stealth layer were chosen to obtain an impedance match, and to diminish the field strength to insignificant values in the allotted stealth layer thickness. When choosing the parameters μ', μ'', σ, and ε for the stealth layer, a great amount of flexibility was found to exist, even when specifying both the stealth layer wave impedance and attenuation per wavelength. The stealth layer was typically one wavelength (15 gridblocks) thick, measured in the stealth material. For this thickness, typically substantially less than 1% of the normally incident power was reflected from the surface of the stealth layer, and the absorbed radiation was reduced to approximately 1% of its original value, before impinging upon the perfectly conducting boundary which is assumed to bound the computational grid. Thinner stealth layers with increased attenuation per wavelength, or thicker stealth layers with less attenuation generally also provide satisfactory results. Our own choice was made for convenience and with a view to not significantly increase computational times. For example, in the case of the monopole in free space ω = 100 MHz, $\mu' = 1.0\mu_0$, $\mu'' = 0.7\mu_0$, σ = 0.00389 S/m, and $\varepsilon = 1.0\varepsilon_0$ in the stealth layer. This matched the free space wave impedance and provided 98.8% attenuation per wavelength.

Simulation results

This section presents some typical results of the thin wire antenna configurations modeled. Simulation results are compared to both experimental and theoretical data. HERZ was implemented in FORTRAN using Macintosh Programmer's Workshop (MPW) version 3.0 on a Macintosh II personal computer, with an RP88 coprocessor to increase performance, which resulted in execution times of approximately six minutes.

Three representative antenna configurations were considered: (1) A bare coaxially fed monopole over an infinite conducting plane operating in a lossless medium, (2) a bare center fed dipole operating in a lossy medium, and (3) a dielectrically coated monopole operating in air. Fig. 4 displays the general configurations modelled in each case.

To validate HERZ, the surface current distribution and input admittance for each antenna configuration were compared to available theoretical or measured values. The boundary condition for the tangential magnetic field at the antenna's surface, $\mathbf{n}\times\mathbf{H} = \mathbf{J}_S$, was used to determine the surface current I, directly from $H_\phi = I/2\pi r$. The driving point admittance was obtained by dividing the current on the antenna nearest the driving point by the voltage across the gap at that point, calculated from $\int \mathbf{E}\cdot\mathbf{dl}$, where $\mathbf{dl}$ is perpendicular or parallel to the antenna axis, depending on whether the gap is coaxial or that of a center fed dipole. Fig. 4 displays the driving points for all configurations. HERZ calculates the fields at the gridblock centers, so to find H_ϕ on the antenna's surface, a third-order polynomial was fitted to the field values in the neighboring blocks, extrapolating radially to the surface. The gridblock configuration in the excitation gaps will be given for each case.

Fig. 5(a) displays the driving point admittance versus antenna length for the monopole in free space. This thin antenna, with $a/\lambda = 0.0064$, and $b/a = 1.189$, was excited at 100 MHz. The theoretical curve, as determined by King (1971, p. 11), was matched very well by the output from HERZ, for all antenna lengths. Fig. 5(b) displays the normalized current distribution along a similar monopole in free space, with $h/\lambda = 0.5$

and $a/\lambda = 0.0254$, also excited at 100 MHz. Here, HERZ agrees closely with the transmission line model by King (1971, p. 18). For both cases, the excitation was specified at the ground plane level, assuming a 1/r coaxial voltage distribution across the gap, with only 2 gridblocks across this region. The formulas used in King's theory (1971, p. 9) rest on the assumption that a TEM mode exists at the junction of the coaxial feed and the antenna, justifying the 1/r excitation used in HERZ.

Fig. 6(a) shows the excellent agreement between HERZ's calculated admittance and Scott's measured values and King's theoretical results (1981 p. 170) for a dipole radiating in a lossy medium, with a conductivity of 5.35×10^{-3} S/m, and relative dielectric constant of 6.0. For this trial, $a/\lambda = 0.00265$, and $a/b = 0.07$, at 114 MHz, where λ, α, and β are the wavelength, attenuation constant, and propagation constant of the radiation in the lossy medium (Ramo and Whinnery 1967). Examination of Fig. 6(a) shows that HERZ provides closer agreement with the measured values than do King's theoretical results.

King assumed a delta function generator in an infinitesimal gap in formulating his theoretical curve, but unfortunately, Scott's gap size is not specified in the forementioned reference. HERZ utilized a gap size (1.0 mm) of the same order as the antenna radius (2.65 mm) for this trial, but several other trials indicate that the gap size is not critical, with results remaining nearly constant for all gap sizes less than the antenna radius. The critical factor in modeling the gap was the number of blocks employed, with four radial and three axial blocks sufficiently representing this sensitive region for the trial represented, as the good results indicated. As the number of gridblocks in this region was decreased, the admittance results deviated from Scott's measured values, but increasing the number of blocks increased the simulation run time, while having insignificant effects on the simulation results. The normalized current distribution for this antenna configuration was also determined using HERZ, for an antenna of length $\beta h = 0.315$. Fig. 6(b) shows the simulation results versus both Scott's measured values and King's theoretical distribution (1981, p. 165).

Experimental results for dielectrically coated antennas by Lamensdorf (1967) were used to verify HERZ in this capacity. Figures 7(a) and 7(b) display Lamensdorf's measured input admittance for a monopole operating in free space at 600 MHz with 2a = 6.35 mm, 2b = 19.05 mm, and D/2a = 3.74, for two different dielectric coatings, $\varepsilon_r = 9.0$ and $\varepsilon_r = 15.0$. Both dielectric coatings were modeled with conductivities of 0.001 S/m. This value was chosen to best represent the non-specific value of $\sigma \leq 0.001$ S/m provided in the Lamensdorf publication. HERZ's simulation results replicate the shape of Lamensdorf's measured distribution, providing a reasonable overall match in both cases. Unlike the monopole previously modeled, in which a TEM coaxial field distribution across the gap could be assumed, the coaxial line was modeled to best represent the actual fields across the gap at the ground plane level. The number of radial gridblocks used to model the coaxial line feeding the antenna depended on the ratio of the outer to inner coaxial radii, b/a. The previous monopole modeled had a b/a value of 1.189 so two grid blocks to represent the gap were sufficient. In the present example, b/a = 3.0, and trial and error indicated that six radial gridblocks were optimal in modeling the gap. TEM excitation was applied at one eighth of a wavelength of the coaxial line below the ground plane. This length of line was modeled in ten axial gridblocks. HERZ's current distribution on a similar antenna configuration with 2a = 6.35 mm, 2b = 19.05 mm and $\sigma = 0.0032$ S/m, but with D/2a = 8, is displayed in Fig. 7(c) along with Lamensdorf's measured values. The agreement is reasonable, but not as good as in previous cases. This may reflect the difficulty of modeling a larger coaxial gap than previously considered, or the inhomogeneity associated with the long dielectric coating.

Additional antenna configurations, radiating into materials ranging from air to highly lossy, were tested along with those cases considered in this paper. Similar agreement with theoretical and measured data was obtained. This agreement was generally comparable to or better than that achieved earlier with a finite element program utilizing radiation boundary conditions (Sumbar *et al.* 1990).

Conclusions

The use of stealth boundary conditions in the finite difference simulation of simple antenna problems appears to be very effective. The method is physically very transparent and the simplicity of the finite difference grid structure permits easy realization of the antenna configurations. The methodology was tested for a monopole in free space, a dipole in a lossy medium, and a dielectrically coated monopole in free space. In all cases, results agreed well with published theoretical and experimentally measured values.

Acknowledgments

The authors wish to acknowledge the financial support of the Natural Sciences and Engineering Research Council of Canada and the help provided by a Faculty of Engineering Dean's Research Award to R.B. Thompson.

References

Albani, M., and Bernardi, P., "A numerical method based on the discretization of Maxwell's equations in integral form," *IEEE Trans. Microwave Theory Tech.*, **MTT-22**, 446 (1974).

Jin, J.M., Volakis, J.L., Liepa, V.V., "An engineer's approach for terminating finite element meshes in scattering analysis," 1991 IEEE AP-S Symposium Digest, vol. 2, pp. 1216-1219, June 1991.

Jin, J.M., Volakis, J.L., Liepa, V.V., "Fictitious absorber for truncating finite element meshes in scattering," *IEE Proc. H*, vol. 139, pp. 472-476, Oct. 1992.

King, R.W.P., *Tables of Antenna Characteristics*, (IFI/Plenum, New York, 1971).

King, R.W.P., *Antennas in Matter: Fundamentals, Theory, and Applications*, (MIT Press, Cambridge, 1981).

Lamensdorf, D., "An experimental investigation of dielectric coated antennas," *IEEE Trans. Antennas Propagat.*, **AT-15**, 767 (1967).

McDonald, B.H., and Wexler, A., "Finite-element solution of unbounded field problems," *IEEE trans. Microwave Theory Tech.*, **MTT-20**, 841 (1972).

Morgan, M.A., Chen, C.H., Hill, S.C., and Barber P.W., "Finite element-boundary integral formulation for electromagnetic scattering," *Wave Motion 6*, 91 (1984).

Nachai, M., Chute, F.S., and Vermeulen, F.E., "On the radio-frequency heating of moist, porous earth-type materials by guided wave propagation along embedded parallel conductors," *J. Microwave Power and Electromagnetic Energy*, 27, No. 3, 143 (1992).

Ramahi, O.M., Khebir, A., and Mittra, R., "Numerically derived absorbing boundary conditions for the solution of open region scattering problems," *IEEE Trans. Antennas Propagat.*, **AP-39**, 350 (1991).

Ramo, S., Whinnery, J.R., and Van Duzer, T., *Fields and Waves in Communication Electronics*, 2nd Ed., (John Wiley & Sons, New York, 1984).

Sumbar, E., Chute, F.S., and Vermeulen, F.E., "A 2-D finite element model for wave propagation into arbitrary inhomogeneous materials," *ACES Journal*, 27 (1990).

Yuan, X., Lynch, D.R., and Strohbehn, J.W., "Coupling of finite element and moment methods for electromagnetic scattering from inhomogeneous objects," *IEEE Trans. Antennas Propagat.*, **AP-38**, 386 (1990).

Figure 1

The general antenna configuration and coordinate system used in HERZ.

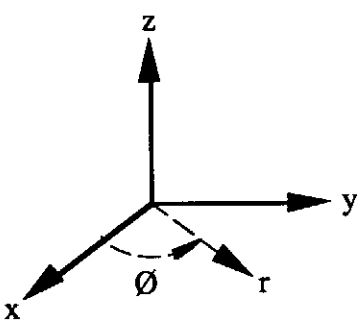

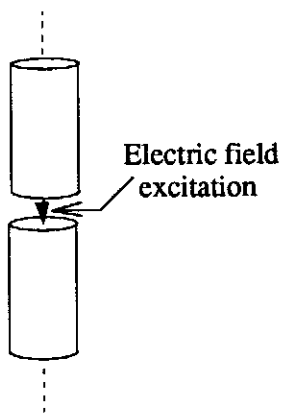

Figure 2

The outline of the finite difference grid system used to model the problem domain and stealth layer. All boundary conditions are specified on the outermost boundary, as indicated.

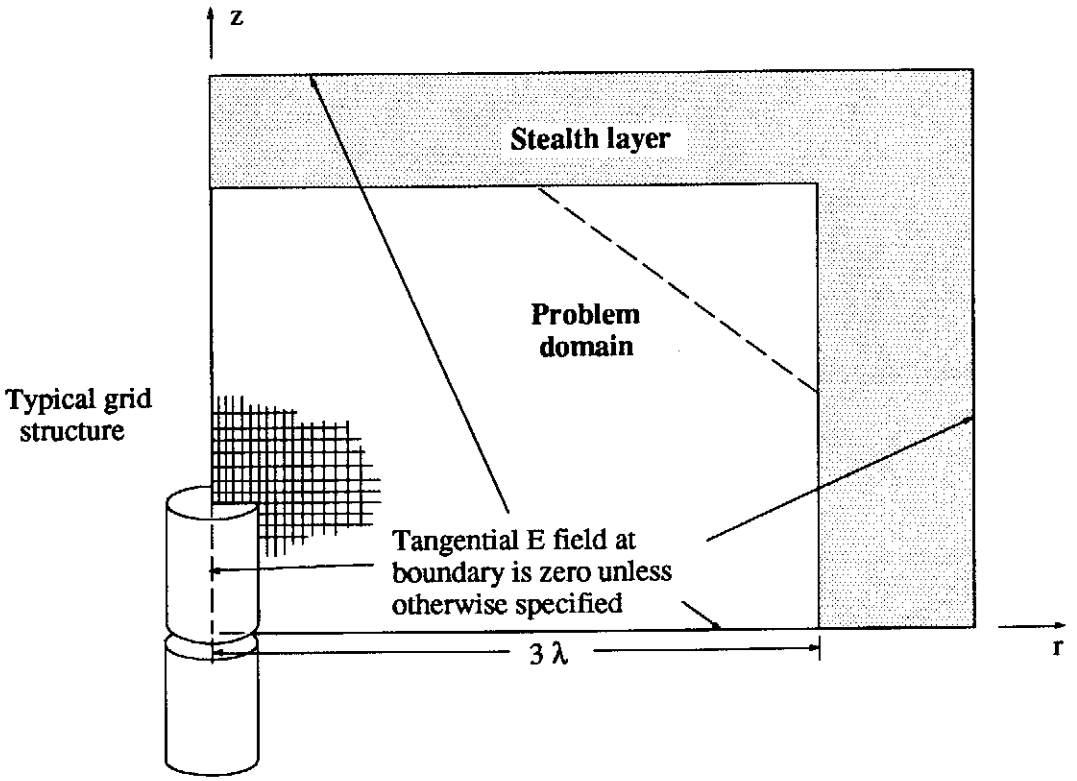

Figure 3

The finite difference grid stucture used in HERZ. All magnetic field components are azimuthally directed and represented at the block centers, while the electric field components are represented on the block boundaries.

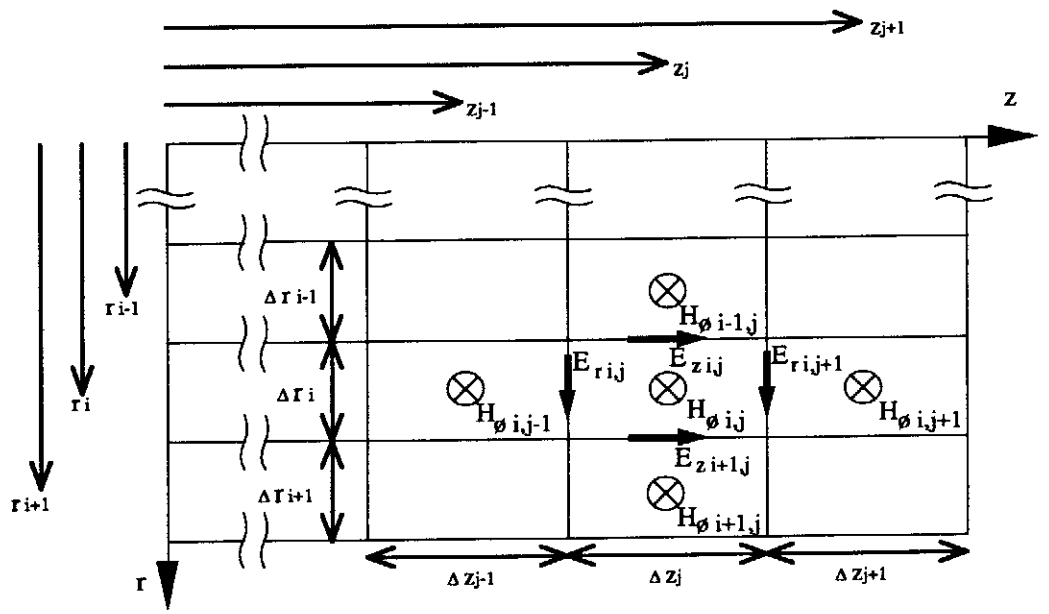

Figure 4

Three antenna configurations modelled with HERZ

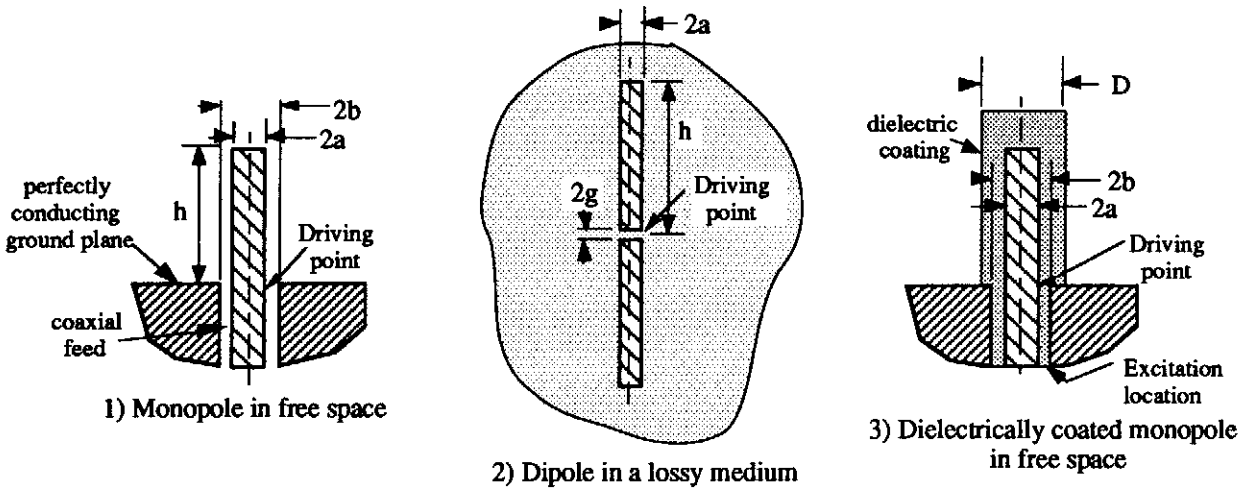

RESULTS

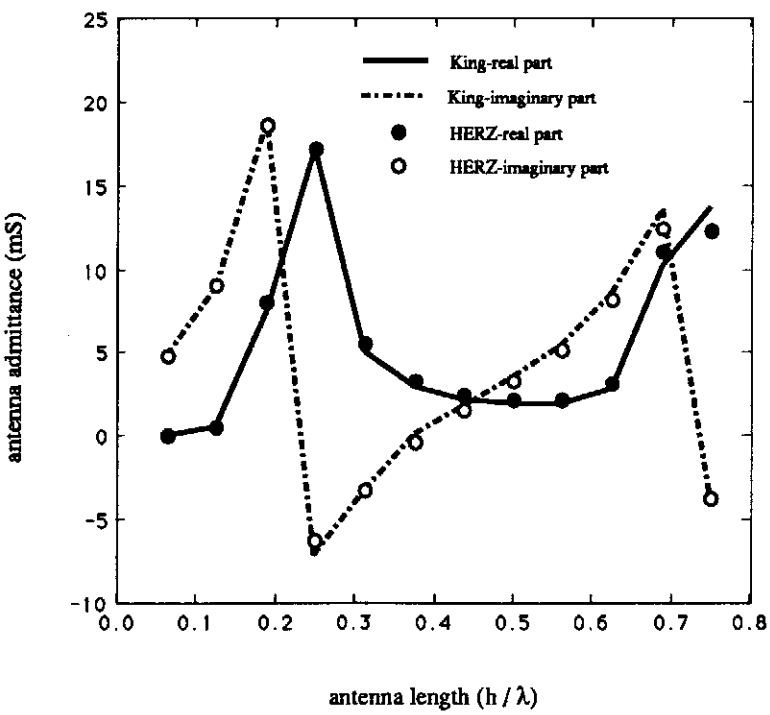

Figure 5(a) Monopole in air

The driving point admittance versus antenna length for a monopole on a conductive plane radiating into a lossless medium. Theoretical data published by King (1971, p.11) is used to validate HERZ's calculated values.

Frequency = 100 MHz

$a / \lambda = 0.0064$

$b / a = 1.189$

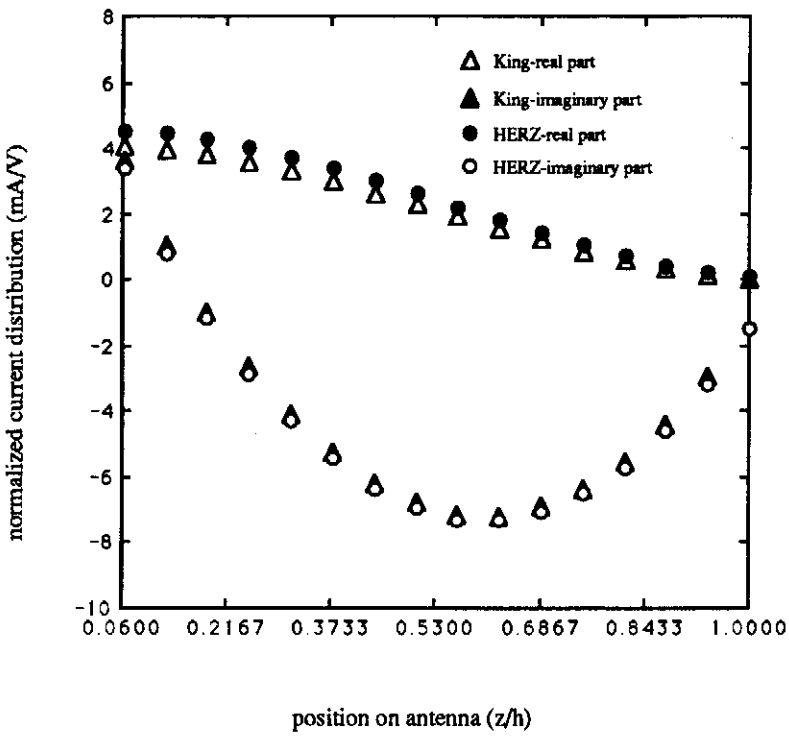

Figure 5(b) Monopole in air

The normalized current distribution for a monopole on a conductive plane radiating into a lossless medium. Theoretical data published by King (1971, p.11) is used to validate HERZ's calculated values.

Frequency = 100 MHz
h / λ = 0.5
a / λ = 0.0254
b / a = 1.189

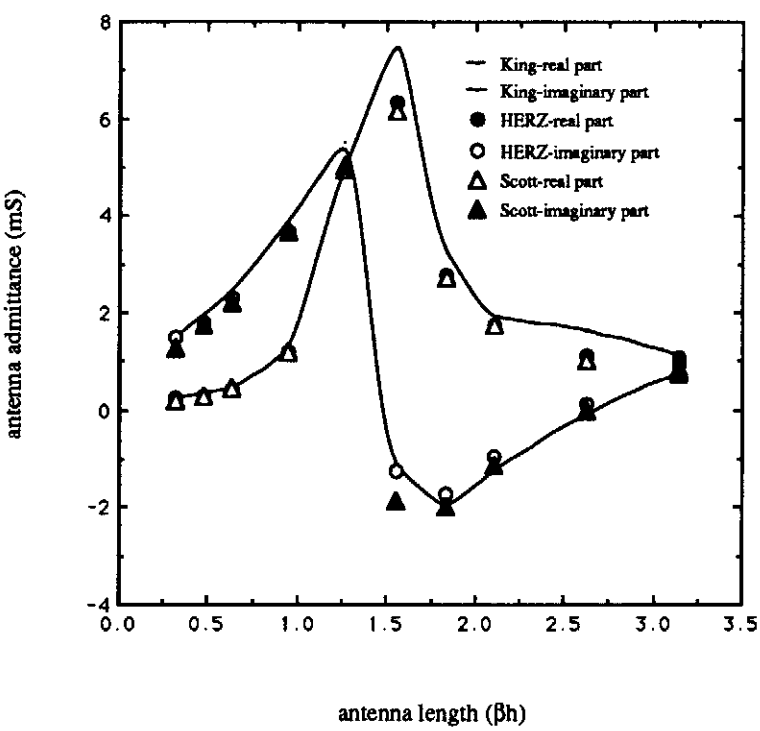

Figure 6(a) Dipole in a lossy medium

The driving point admittance versus antenna length for a dipole operating in a lossy medium as measured by Scott, theoretically determined by King (1981, p. 170), and calculated with HERZ.

Frequency = 114 MHz
a / λ = 0.0265
α / β = 0.07

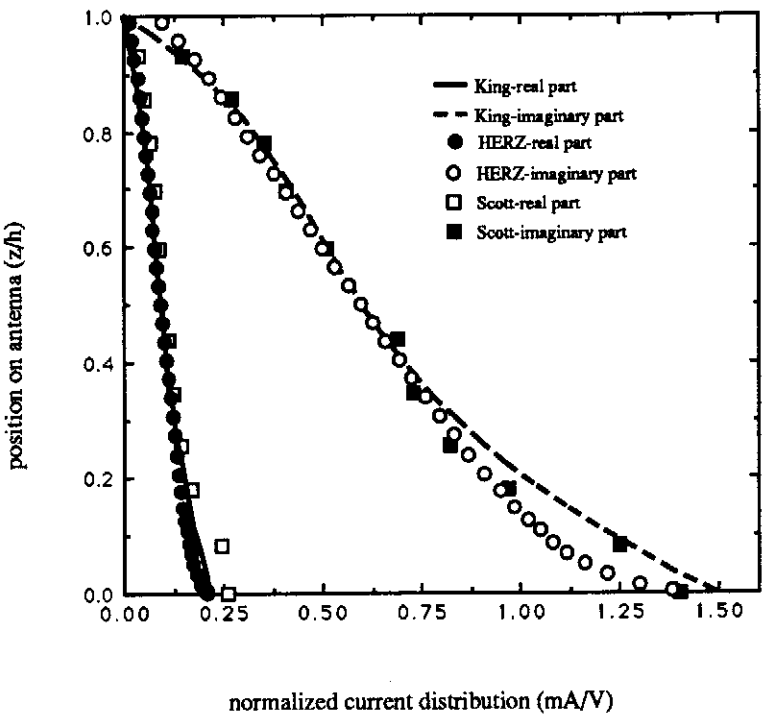

Figure 6(b) Dipole in a lossy medium

HERZ's normalized current distribution for a dipole radiating into a lossy medium is compared to theoretical data by King (1981, p.165) and the measured values by Scott.

Frequency = 114 MHz
$\beta\lambda$ = 0.315
a / λ = 0.0265
α / β = 0.07

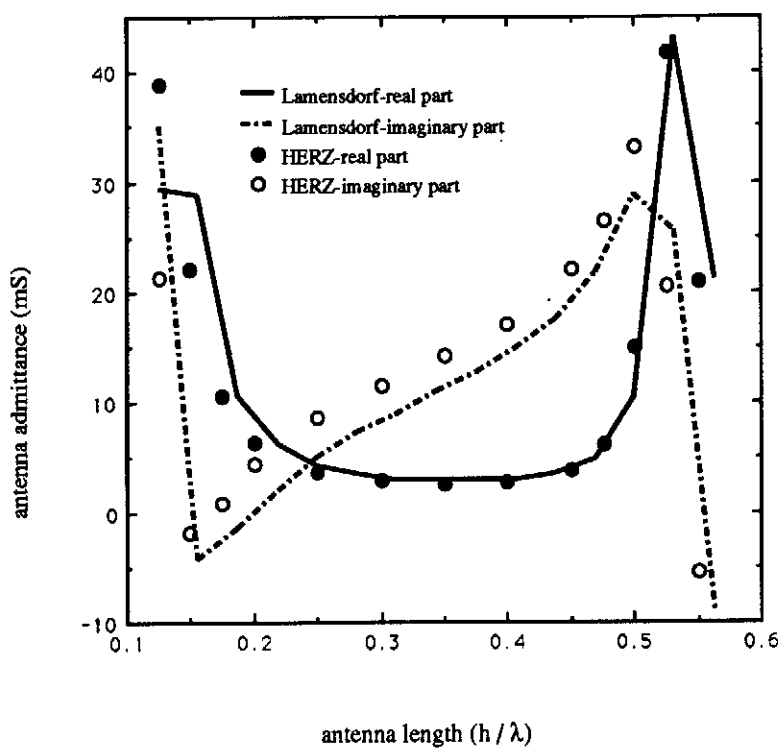

Figure 7(a) Dielectrically coated monopole in air

The driving point admittance versus antenna length for a dielectrically coated monopole in air as measured by Lamesndorf (1967) and calcualted with HERZ.

Frequency = 600 MHz
$2a$ = 6.35 mm
$2b$ = 19.05 mm
D = 23.77 mm
ε_r = 9
σ = 0.001 S / m

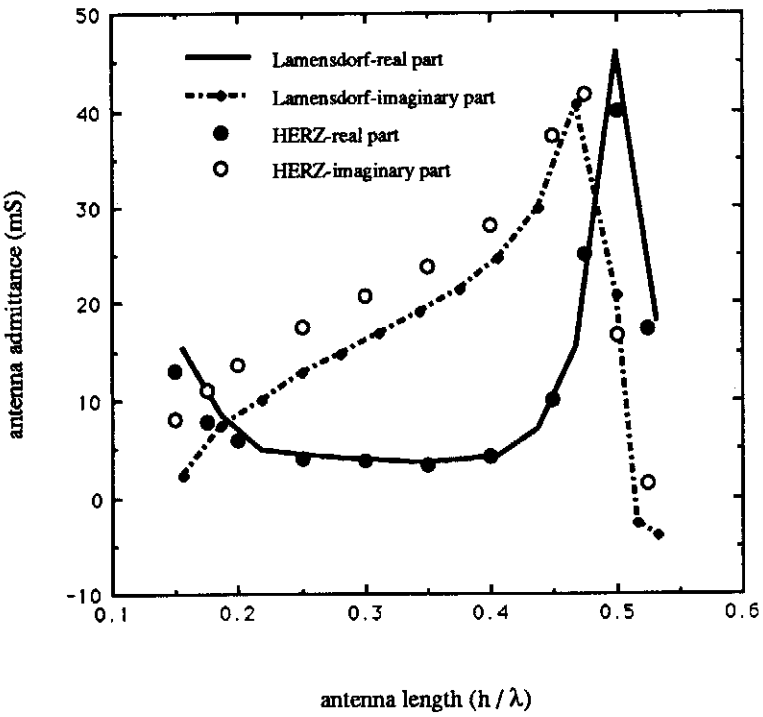

Figure 7(b) Dielectrically coated monopole in air

The driving point admittance versus antenna length for a dielectrically coated monopole in air as measured by Lamensdorf (1967) and calculated by HERZ.

Frequency = 600 MHz
$2a$ = 6.35 mm
$2b$ = 19.05 mm
D = 23.77 mm
ε_r = 15
σ = 0.001 S / m

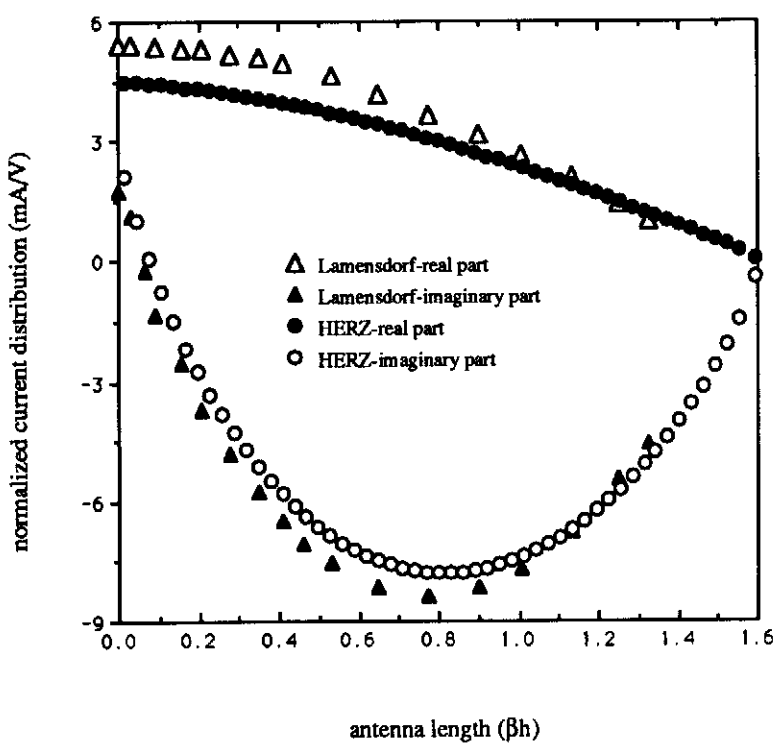

Figure 7(c) Dielectrically coated monopole in air

The normalized current distribution for a dielectrically coated monopole on a conducting plane operating in air. HERZ's calculated values are compared to Lamensdorf's measured values (1967).

Frequency = 600 MHz
$2a$ = 6.35 mm
$2b$ = 19.05 mm
D = 50.79 mm
ε_r = 3.2
σ = 0.0032 S / m